

Research Article

doi.org/10.1002/prep.202100106

A Statistical Hot Spot Reaction Rate Model for Shock Initiation of Polymer-Bonded Explosives

Zhi-ling Bai,^[a] Zhuo-ping Duan,^{*[a]} Xin-jie Wang,^[a] and Feng-lei Huang^{*[a]}

Abstract: A statistical hot spot reaction rate model for shock initiation and detonation of heterogeneous solid explosives is developed to devote a physically realistic description of the formation, growth, or coalescence of hot spots, combustion, and rapid transition to detonation. One of the most significant advantages of the statistical model is that it predicts well the influence of mesoscopic void size distribution and critical size of activated hot spots on the shock initiation and detonation growth of PBXs. The calculated pressure histories in both TATB-based LX-17 and HMX-based PBX9501 are found to be in good agreement

with the experimental data. It is found that the shock initiation behavior of the HMX-based PBX is mainly controlled by the number density of hot spots and shows an accelerated reaction characteristic and that of the TATB-based PBX is determined by the combustion reaction process, which featured by a stable reaction characteristic. It is also found that the void size inside the explosive should be restricted as small as possible to effectively reduce the initiation sensitivity. The results could advance our knowledge of shock initiation of PBXs and provide guidelines for the synthesis of insensitive high composite explosives.

Keywords: shock initiation · PBX explosives · void size distribution · statistical hot spot reaction rate model

1 Introduction

Investigations into the shock initiation mechanisms and the detonation growth behaviors of a heterogeneous solid explosive under shock loadings have been a critical issue in practical military and civil engineering applications for a long time, in which a key problem is to choose an available reactive flow model for the explosives, including the calibration of the model parameters, to quantitatively and accurately predict the shock initiation and subsequent detonation growth processes in the explosives.

For a polymer-bonded explosive (PBX), the shock initiation behavior is significantly different from that of the homogeneous solid explosive due to the mesostructure heterogeneity, which consists of explosive particles with various sizes and shapes, and some randomly distributed pore defects. As a result, the shock initiation and detonation growth behaviors of PBXs is highly complicated and affected by many factors, namely the explosive component [1–3], external confinement [4], ambient temperature [5–7], and loading pressure [8–10], as well as the mesostructure characteristics such as the size distributions of explosive grains [11–13] and void defects [14]. These detailed studies have provided useful insight into a closer description and accurate prediction of the shock initiation behaviors. However, to date, the detail of the mesoscopic physical mechanisms of shock initiation in heterogeneous solid explosives has not yet been fully understood, and relatively few reactive flow models can be used to estimate the influence of mesostructure of heterogeneous solid explosives on shock initiation behaviors.

It has been suggested that significantly high temperature localized at defects in heterogeneous solid explosives, which further leads to the formation of "hot-spot" and even initiation. A multitude of studies showed that pore collapse is a dominant hot-spot mechanism for shock initiation of pressed solid explosives [6, 11–12]. Recently, Duan et al. [12, 15–19] proposed an elastic/viscoplastic pore collapse "hot-spot" model and then developed a Duan-Zhang-Kim (DZK) mesoscopic reaction rate model, which can well delineate the effects of initial temperature, loading pressure, particle size, porosity, and binder's content/strength on shock initiation and detonation growth of PBXs. Up to now, the DZK model is generally accepted due to the advantage that fewer parameters in the DZK model need to be determined compared with the most commonly used ignition and growth model (IG) developed by Lee and Tarver [20]. However, the hot-spot ignition term in DZK model assumes that there are plenty of hot spots and all hot spots are similar, therefore, a representative homogenized spherical pore collapse cell was used to describe the hot-spot ignition of explosives. Thus the hot-spot ignition term in DZK model can do little for estimating the effects of size distribution of voids and crystals on the shock initiation behavior of PBXs.

On the other hand, some statistical hot spot reaction rate models (SHSM) have been developed to describe the

[a] Z.-l. Bai, Z.-p. Duan, X.-j. Wang, F.-l. Huang
State Key Laboratory of Explosion Science and Technology, Beijing Institute of Technology, Beijing 100081, China

*e-mail: duanzp@bit.edu.cn
huangfl@bit.edu.cn

influence of voids size distribution on the number density of hot spots in shocked explosives, such as the three-factor model of Grebenkin [21], Cochran model [22], Nichols-Tarver model [23], Gambino-Nichols model [24], Hill model [25] and Hamate-Horie model [26,27]. These statistical models allow for a closer physically realistic description of hot spot generation, growth, and coalescence, as well as the quench of locally heated regions due to the thermal dissipation at the hot spot ignition stage. However, compared with the high-fidelity computing of hot-spot ignition reaction, the simple laminar burning mechanism is generally employed to illustrate subsequent combustion reaction and rapid transition to detonation in most current SHSM-type reaction rate models. As a result, these models could not well describe the experimental data, especially the pressure at the detonation stage [28]. The reason is that the combustion topology at the low-pressure slow combustion stage is much different from that of the high-pressure detonation reaction stage, depending on the distinct reaction mechanism. At the initial stage of shock initiation, the combustion topology is characterized by the density of reacted hot spots, the combustion wave speed, and geometric topology. While at the detonation stage, the density of hot spots becomes saturated due to the high loading pressure, and the detonation is dominated by the rapid thermal explosion mechanism.

The present work aims at investigating the distinct reaction mechanisms at different reaction stages for shock initiation and detonation growth in PBXs. A statistical hot spot reaction rate model is developed to investigate the effect of void size distribution on hot spot ignition. This paper is divided into five sections as follows. After this brief introduction, the void size distribution characteristic is presented in Section 2. In Section 3, the statistical hot spot reaction rate model is proposed, and the numerical simulations and experimental data are summarized in Section 4, together with some discussions. Finally, some conclusions are drawn out in Section 5.

2 Void Size Distribution in PBXs

It is widely recognized that void size distribution in the explosive is mainly related to the particle size distribution and granularity of the explosive component. Willey et al. [14] carried out the ultra-small angle X-ray scattering (USAXS) experiments to obtain the void size distribution of PBX explosives and found that the void size in TATB-based explosives LX-17 shows a bimodal distribution, as shown in Figure 1(a). Fits of the USAXS data is given by a function as,

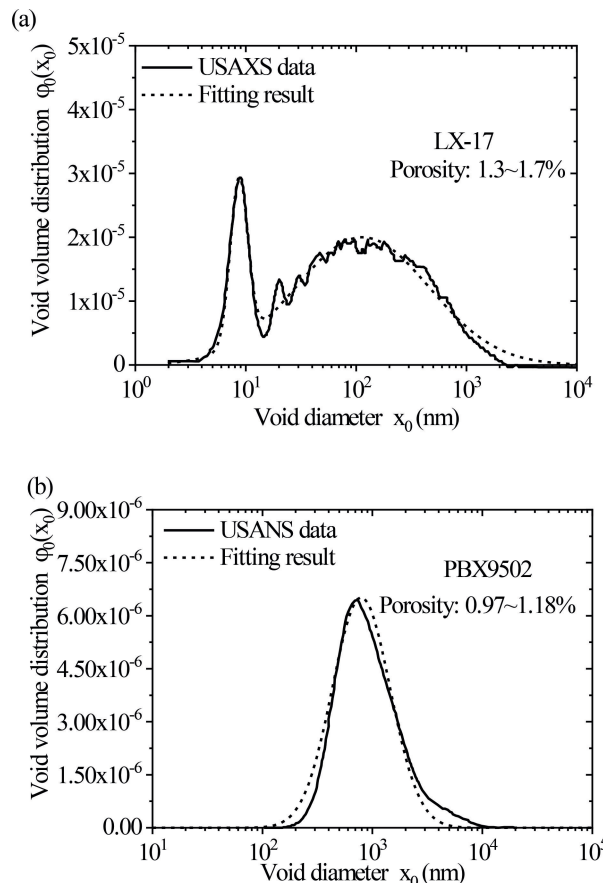


Figure 1. Void size distribution in LX-17 and PBX9501 are characterized by the bimodal/unimodal distribution

$$\begin{aligned} \varphi_0(x_0) = & a_1 \exp \left[\frac{-(\log(x_0) - c_1)^2}{2\omega_1^2} \right] \\ & + a_2 \exp \left[\frac{-(\log(x_0) - c_2)^2}{2\omega_2^2} \right] \end{aligned} \quad (1)$$

where a_1 and a_2 are amplitudes, c_1 and c_2 are location parameters, and ω_1 and ω_2 are shape parameters, respectively. Moreover, as shown in Figure 1(b), Mang et al. [29] measured and observed one peak in the void size distribution of HMX-based PBX9501 using the ultra-small angle neutron scattering (USANS) method. Then we determined the parameter values by fits to the USANS data using the Eq. (1) to facilitate the following hot spot ignition modeling. Table 1 summarized the values of a parameter of void size distribution in LX-17 [14] and PBX9501.

3 The SHS-DZK Reaction Rate Model

Compared with size of initial void x_0 , the size of "hot spot" x is much smaller (almost by an order of magnitude), and it is usually simply assumed that,

Table 1. Parameters of the void size distribution in LX-17 and PBX9501.

Parameters	LX-17[14]	PBX9501
a_1/nm^{-1}	2.58e-5	6.53e-6
$10^{c1}/\text{nm}$	8.7	790.0
$10^{\omega1}/\text{nm}$	1.2	1.83
a_2/nm^{-1}	2.00e-5	
$10^{c2}/\text{nm}$	114.0	
$10^{\omega2}/\text{nm}$	4.04	

$$x = \beta x_0 \quad (2)$$

where $\beta \approx 0.1$ [21]. Substitution of Eq. (2) into Eq. (1) gives the size distribution of potential hot spots (locally heated regions) as,

$$\varphi(x) = \beta^2 \left\{ a_1 \exp \left[-\frac{(\log(x/\beta) - c_1)^2}{2\omega^2} \right] + a_2 \exp \left[-\frac{(\log(x/\beta) - c_2)^2}{2\omega_2^2} \right] \right\} \quad (3)$$

Based on the statistical treatment of hot spots reaction in Cochran's model [22], it is assumed that there are potential spherical heated regions with radius of r and number of $M(t, r)\Delta r$ per unit volume of explosives appear at time t under shock loading. After that, some heated regions become dead and completely extinct due to thermal dissipation, and the rest is activated/reacted and generated spherical reaction nuclei with radius of r and number of $N(t, r)\Delta r$. In this way, the hot-spot ignition reaction degree per unit volume of explosives is defined as

$$\lambda_{h,\text{statistics}} = \int_{d_{cr}/2}^{\infty} \frac{4\pi}{3} r^3 N(r, t) dr \quad (4)$$

Note that the lower limit of integration in Eq. (4) takes the critical size of reacted hot spot d_{cr} (μm) into account, and the size of d_{cr} depends on the hot spot temperature T and pressure of shock precursor P_f , which is given by [21]

$$d_{cr} = \left(\frac{T_1}{T_0 + bP_f} \right)^{\frac{1}{\gamma}} \quad (5)$$

where T_0 is the initial temperature, T_1 , b and γ are the thermodynamic constants, respectively. For TATB, $T_1 \approx 1400$ K, $b = 200$ K/GPa, $\gamma \approx 0.08$ [6]. For HMX, $T_1 \approx 1000$ K, $b = 150$ K/GPa, $\gamma \approx 0.06$.

Furthermore, the statistical kinetic equations for potential hot spots and reaction nuclei are given by [22]

$$\frac{\partial M}{\partial t} = \dot{S}(r) - \frac{DM}{r^2} - KM \quad (6)$$

$$\frac{\partial N}{\partial t} = KM - v \frac{\partial N}{\partial r} \quad (7)$$

where $\dot{S}(r)$ is the source rate of locally heated regions, D is the thermal diffusivity, K is the rate at which the heated sites into a reaction nucleus and v is the growth velocity of the reaction nucleus, respectively. Here, $v = v_0 p$, p is the real-time pressure, and v_0 is a constant.

To capture the main features of the dominant mechanism of hot spot formation, i.e. void collapse, during the shock initiation process of heterogeneous solid explosives, the nucleation rate K is given by a phenomenological formula as follow [23],

$$K = \left(\frac{AP^*(p - P_c)}{P^* + p - P_c} \right) H(p - P_c) \quad (8)$$

where A is a constant, and P_c is the threshold pressure of ignition, which represents the resistance to void collapse. To avoid an unrealistically large collapse rate, P^* is defined as the saturation pressure. H is the Heaviside step function.

The source rate $\dot{S}(r)$ is denoted using the following expression [22],

$$\dot{S}(r) = \begin{cases} -f(r) \dot{V} \left(1 - \frac{4\pi}{3S_{\max}} \int_{d_{cr}/2}^{\infty} S r^3 dr \right), & \dot{V} < 0 \\ 0, & \dot{V} \geq 0 \end{cases} \quad (9)$$

where S_{\max} is a scale parameter restricting the total volume that can be heterogeneously heated. It is generally presumed that S_{\max} was determined by the initial porosity, $S_{\max} = 1 - \rho_0 / \rho_{\text{TMD}}$, where ρ_{TMD} is the theoretical density. $f(r)$ is the number distribution function of potential spherical hot spots, which can be derived by Eq. (3):

$$f(r) = \frac{\beta^2}{\frac{4\pi r^3}{3}} \left\{ a_1 \exp \left[-\frac{(\log(2r/\beta) - c_1)^2}{2\omega^2} \right] + a_2 \exp \left[-\frac{(\log(2r/\beta) - c_2)^2}{2\omega_2^2} \right] \right\} \quad (10)$$

The governing equations (6) and (7) for hot spot ignition reaction can be solved with the method of moments [22]. Let

$$\langle Mr^n \rangle = \int_{d_\sigma/2}^{\infty} Mr^n dr$$

$$\langle Nr^n \rangle = \int_{d_\sigma/2}^{\infty} Nr^n dr$$

Then an approximate method is adopted as

$$\langle Mr^{-2} \rangle \simeq \frac{9}{2} \frac{\langle M \rangle^3}{\langle Mr \rangle^2}$$

$$\langle Mr^{-1} \rangle \simeq \frac{3}{2} \frac{\langle M \rangle^2}{\langle Mr \rangle}$$

Thus, Eqs. (6) and (7) becomes

$$\begin{aligned} \frac{d\langle M \rangle}{dt} &= \langle \dot{S} \rangle - \frac{9}{2} D \frac{\langle M \rangle^3}{\langle Mr \rangle^2} - K \langle M \rangle \\ \frac{d\langle Mr \rangle}{dt} &= \langle \dot{S}r \rangle - \frac{3}{2} D \frac{\langle M \rangle^2}{\langle Mr \rangle} - K \langle Mr \rangle \\ \frac{d\langle Mr^2 \rangle}{dt} &= \langle \dot{S}r^2 \rangle - D \langle M \rangle - K \langle Mr^2 \rangle \\ \frac{d\langle Mr^3 \rangle}{dt} &= \langle \dot{S}r^3 \rangle - D \langle Mr \rangle - K \langle Mr^3 \rangle \end{aligned} \quad (13)$$

$$\begin{aligned} \frac{d\langle N \rangle}{dt} &= K \langle M \rangle \\ \frac{d\langle Nr \rangle}{dt} &= (K \langle Mr \rangle + v \langle N \rangle) \left(1 - \frac{\langle Nr \rangle}{Q} \right) \\ \frac{d\langle Nr^2 \rangle}{dt} &= (K \langle Mr^2 \rangle + 2v \langle Nr \rangle) \left(1 - \frac{\langle Nr^2 \rangle}{Q^2} \right) \\ \frac{d\langle Nr^3 \rangle}{dt} &= (K \langle Mr^3 \rangle + 3v \langle Nr^2 \rangle) \left(1 - \frac{4\pi}{3} \langle Nr^3 \rangle \right) \end{aligned} \quad (14)$$

Where,

$$\begin{aligned} \langle \dot{S} \rangle &= Y \langle f(r) \rangle \\ \langle \dot{S}r \rangle &= Y \langle f(r)r \rangle \\ \langle \dot{S}r^2 \rangle &= Y \langle f(r)r^2 \rangle \\ \langle \dot{S}r^3 \rangle &= Y \langle f(r)r^3 \rangle \end{aligned} \quad (15)$$

$$Y = -\dot{V} \left(1 - 4\pi \langle Sr^3 \rangle / 3S_{\max} \right) \quad (16)$$

$$(11) \quad Q = \left[3 \langle N \rangle^2 / 4\pi \right]^{1/3}$$

$$(17)$$

Finally, the reaction rate and reaction degree of ignition per unit volume of explosive can be obtained as,

$$\left(\frac{d\lambda}{dt} \right)_{h,\text{statistics}} = \frac{4\pi}{3} \frac{d\langle Nr^3 \rangle}{dt} \quad (18)$$

$$(12)$$

$$\lambda_{h,\text{statistics}} = \frac{4\pi}{3} \langle Nr^3 \rangle \quad (19)$$

Therefore, the thermodynamic parameters to be determined in the hot-spot ignition term are T_1 , b , γ , v_0 , A , P^* , and P_c .

As the hot-spot ignition reaction evolves, the explosive enters the early low-pressure slow reaction stage, which is usually described by the surface combustion mechanism. Then the explosive maybe enters a high-pressure fast reaction stage and transition to detonation. A series of studies shows that the DZK reaction rate model [12, 16, 28] has some success in describing slow reaction stage and fast reaction process. Therefore, based on the DZK model [28], a statistical hot spot DZK-type (SHS-DZK) model is built as

$$\frac{d\lambda}{dt} = \left(\frac{d\lambda}{dt} \right)_{h,\text{statistics}} + \frac{3\lambda^{2/3}(1-\lambda)^b}{r_{o,\text{statistics}}} ap^n + Gp^m(1-\lambda)^s \quad (20)$$

where $\lambda_{h,\text{statistics}}$ is the hot-spot ignition reaction degree (see Eqs. (4) and (19)), $r_{o,\text{statistics}}$ stands for the statistical mean granularity of explosive component (μm); λ and p are the total reaction degree of the explosive (i.e. the total volume fraction reacted) and real-time pressure (Mbar) at time t ; a , b , G , m , n , and s are all constants determined by fitting the numerical results to a shock initiation experimental data. The first term describes the nucleation reaction process of the "hot spot", the second term presents the low-pressure slow combustion process once the hot spot is ignited, and the third term is a high-pressure fast reaction phase [30] to describe the overall detonation reaction in explosives.

Moreover, the total reaction degree λ can be obtained by integrating Eq. (20), which in general is written as,

$$\lambda = \lambda_{\text{ignition}} + \lambda_{\text{slow}} + \lambda_{\text{fast}} \quad (21)$$

where $\lambda_{\text{ignition}}$, λ_{slow} , and λ_{fast} represent in turn the contribution of the hot-spot ignition term, the low-pressure slow reaction term, and the high-pressure fast reaction term, respectively. Eq. (21) allows for the evaluation of different reaction mechanisms at different reaction stages for the shock initiation and detonation growth processes in the explosives.

4 Results and Discussion

The SHS-DZK model is incorporated into a hydrodynamic code DYNA2D to simulate the 1D shock initiation and the detonation growth of HMX-based PBX9501 (95% HMX, 2.5% Estane, 2.5% BDNPA-F nitroplasticizer) and TATB-based LX-17 (92.5% TATB, 7.5% Kel-F). The parameter values of the hot-spot ignition term and the last two terms [18] of the SHS-DZK model are listed in Table 2 and Table 3, respectively.

A mesh resolution of 25 μm is sufficient to reach convergence for the shock pressure, with further mesh refinement down to 10 μm resulting in relative fluctuations of 2.1%. The artificial viscosity method developed by Lands-hoff [31] for shock capturing and the hourglass type viscosity force to stabilize the grid by reducing spurious distortions are used for Lagrangian finite difference algorithm. Moreover, it is important to explain that this study is fo-

cused on the macro-scale shock initiation and detonation behavior of the explosive, not on the details of local fields, in which a finer mesh resolution would likely be required to accurately resolve local temperature, as is commonly the case for small-scale simulations.

In addition, temperature-dependent Jone-Wilkins-Lee (JWL) equations of state (EOS) is adopted for both detonation products and unreacted explosives [32] as

$$p = A e^{-R_1 \bar{V}} + B e^{-R_2 \bar{V}} + \frac{\omega c_v}{\bar{V}} T \quad (22)$$

where, p , \bar{V} and T are the pressure (Mbar), relative specific volume and temperature (K), respectively. A , B , R_1 , R_2 , ω and c_v are constants. The values of parameters in Eq. (22) for PBX9501 and LX-17 [1, 32] are summarized in Table 4.

The typical experimental data [2, 32] and the calculated pressure histories at several Lagrangian locations in PBX9501 and LX-17 are presented in Figure 2. A satisfactory agreement is seen between the numerical results and the experimental data, which implies that the SHS-DZK model can preferably describe the shock initiation and detonation of PBXs. It is worth noting that the calculated detonation transition time is slightly earlier than the experimental results of the LX-17 samples, which may arise from the different void size distributions by differences of preparation methods and particle size distribution, etc.

To further analyze the mechanisms of shock initiation of HMX-based PBX9501 and TATB-based LX-17, the reaction degree histories at different Lagrangian locations are shown in Figure 3 and Figure 4, and the histories of ignition term $\lambda_{\text{ignition}}$, low-pressure slow reaction term λ_{slow} and high-pressure fast reaction term λ_{fast} are also extracted, respectively. It is found that the reaction degree profile reproduces well the build-up to detonation. For PBX9501, the contribution of combustion reaction at the low-pressure slow reaction stage λ_{slow} is more, which indicates that the initiation of HMX-based PBXs is dominated by accelerated reaction after ignition. On the contrary, for LX-17, there is a relatively small λ_{slow} increasing due to the lower temperature of gaseous products of TATB [21], suggesting that the shock ini-

Table 2. Thermodynamic parameters of the hot-spot ignition term of the SHS-DZK model for PBX9501 and LX-17.

Parameters	PBX9501	LX-17
T_1/K	1000.0	1400.0
$b/(\text{K}\cdot\text{GPa}^{-1})$	150.0	200.0
γ	0.06	0.08
$D/(\text{cm}^2\cdot\mu\text{s}^{-1})$	1.0e-10	1.0e-10
$v_0/(\text{cm}\cdot\mu\text{s}^{-1}\cdot\text{GPa}^{-1})$	3.0e-3	1.8e-3
$A/\mu\text{s}^{-1}$	2000.0	2000.0
P^*/GPa	40.0	40.0
P_c/GPa	2.0	3.0

Table 3. Parameters of the second and the third terms of the SHS-DZK model for PBX9501 and LX-17[18].

Parameters	PBX9501	LX-17
a	0.027	0.01
b	2.05	1.70
n	1.00	2.03
G	800.0	220.0
m	3.355	3.077
s	1.00	0.2

Table 4. Parameters of the JWL EOS for the detonation products and unreacted explosives of PBX9501 and LX-17[1, 32].

Parameters	PBX9501[32]		LX-17[1]	
	Detonation Products	Unreacted Explosives	Detonation Products	Unreacted Explosives
A/Mbar	16.689	7320.0	13.454	632.07
B/Mbar	0.5969	-0.052654	0.6727	-0.04472
R_1	5.9	14.1	6.2	11.3
R_2	2.1	1.41	2.2	1.13
ω	0.45	0.8867	0.5	0.8938
$c_v/(\text{Mbar}\cdot\text{K}^{-1})$	1.0e-5	2.7806e-5	1.0e-5	2.487e-5
E_0/Mbar	0.102	-	0.069	-

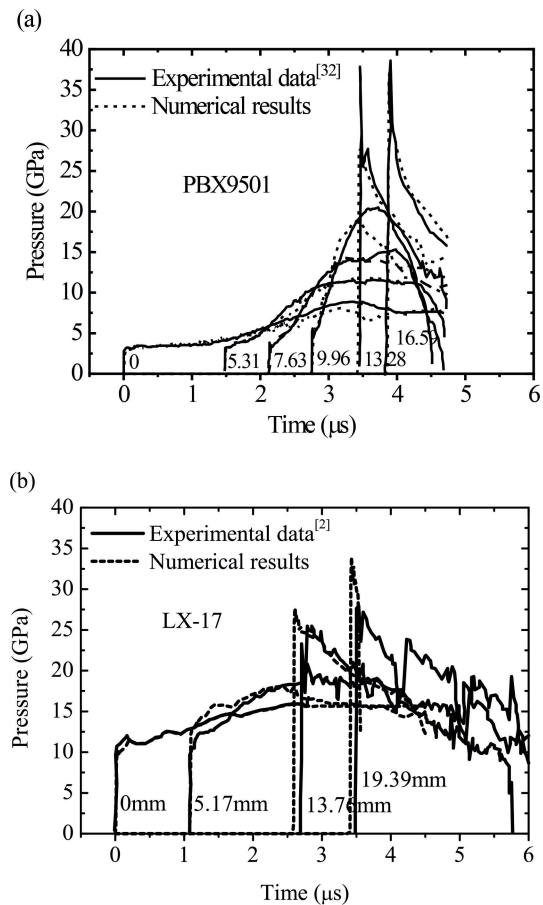


Figure 2. Experimental data and numerical results for the pressure growth histories in PBX9501 and LX-17. (a)PBX9501, (b) LX-17.

tiation of TATB-based PBXs presents a stable reaction behavior.

As shown in Figure 5, the higher the loading pressure, the faster the chemical reaction rate of PBX9501. The remarkably higher hot-spot ignition rate localize near the shock front. The results can be better explained from Eq. (5) that the higher the pressure, the smaller the critical size of reacted hot spot, and there are more reacted hot spots contribute to the ignition and combustion stages. In addition, it should be pointed out here that the hot-spot ignition plays a dominant role at low pressure, while at high pressure, the density of hot spots may be saturated, and thus the shock initiation is dominated by the combustion process. Moreover, as shown in Figure 6, the higher the initial temperature, the more activated hot spots, and the faster the hot-spot ignition. It is worth noting that the ignition reaction degree is about 1% [20] when the hot-spot ignition stage is completed in the hot-spot ignition term of DZK model.

The PBX9501 with a density of $\rho_0 = 1.84 \text{ g/cm}^3$ ($\rho_{\text{TMD}} = 1.86 \text{ g/cm}^3$) and five different kinds of void size distribution are used to investigate the influence of void size distribution on the shock ignition sensitivity and initiation be-

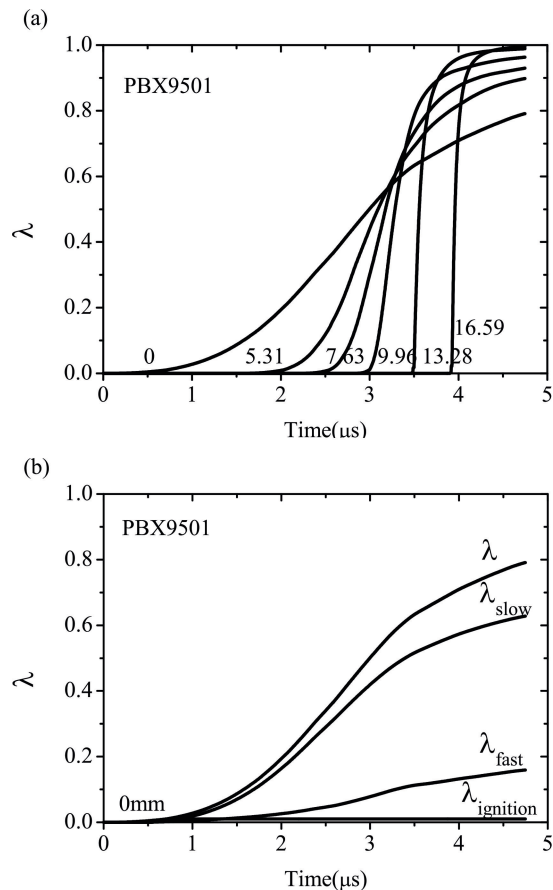


Figure 3. Typical reaction degree histories of shock initiation in PBX9501. (a) Overall reaction degree histories at different Lagrangian locations, (b) reaction degree contribution of the hot-spot ignition term, the slow combustion term and the fast reaction term at 0 mm.

havior of PBXs, as shown in Figure 7, and Table 5 summarized the parameter values of the five kinds of void size distribution (see Eq. (1)) in PBX9501 with the same porosity. The present paper mainly focuses on general trends rather than quantitative results and examining whether the calculated results are consistent with commonly held ideas about shock ignition and sensitivity of porous explosives. Thus except for the data of No. 2 measured with USANS (see Table 1), the rest four are artificially set and modified

Table 5. Parameters for five different kinds of void size distribution in PBX9501 with the same porosity.

No.	a_1/nm^{-1}	$10^{c1}/\text{nm}$	$10^{w1}/\text{nm}$
1	8.544e-6	590.0	1.83
2 [22]	6.530e-6	790.0	1.83
3	3.916e-6	790.0	2.33
4	2.651e-6	790.0	2.83
5	2.100e-6	2456.0	1.83

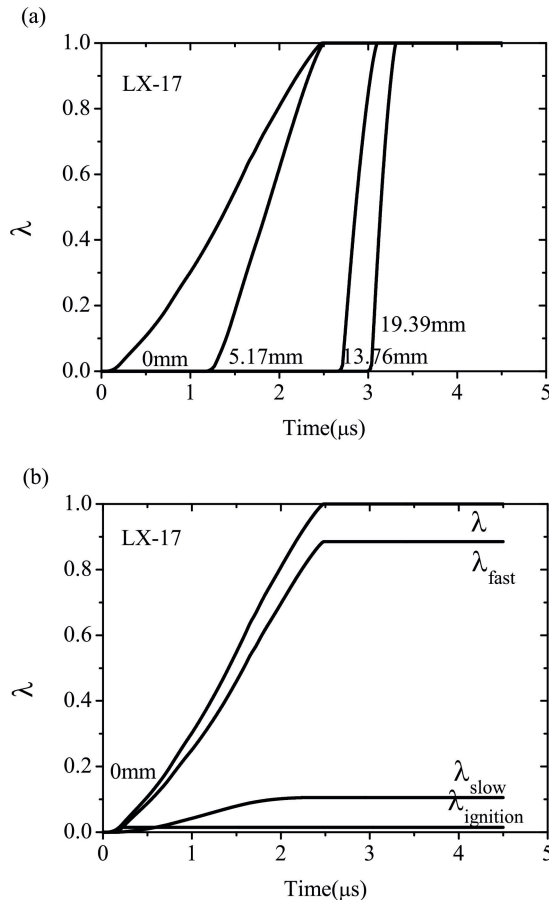


Figure 4. Typical reaction degree histories of shock initiation in LX-17. (a) Overall reaction degree histories at different Lagrangian locations, (b) Reaction degree contribution of the hot-spot ignition term, the slow combustion term and the fast reaction term at 0 mm.

for the evaluation purpose. It can be seen that compared with No. 2, No. 1 has more smaller-sized voids, and No. 5 has more large-sized voids, while No. 3 and No. 4 are more dispersed in size.

Figure 8 shows the calculations of effects of void size distribution on the shock ignition behavior of PBX9501 under the same loading pressure, wherein (a) and (b) are the histories of overall reaction degree and hot-spot ignition term, (c) and (d) are the hot-spot ignition rate peaks changing with the key parameters 10^{ω_1} and 10^{ϵ_1} for the distribution characteristics. It is found that the explosive with both smaller voids (No. 1) and larger voids (No. 5) exhibit the lowest ignition reaction rate because few hot spots are activated in these two cases. Moreover, the more dispersed the void size distribution (No. 4 > No. 3 > No. 2), the lower the ignition reaction rate. When the void size distribution is more dispersed, more voids will be too small to be activated as hot spots, which results in a slower ignition reaction rate. In the practical preparation of ammunition charge, the defect size inside the explosive should be re-

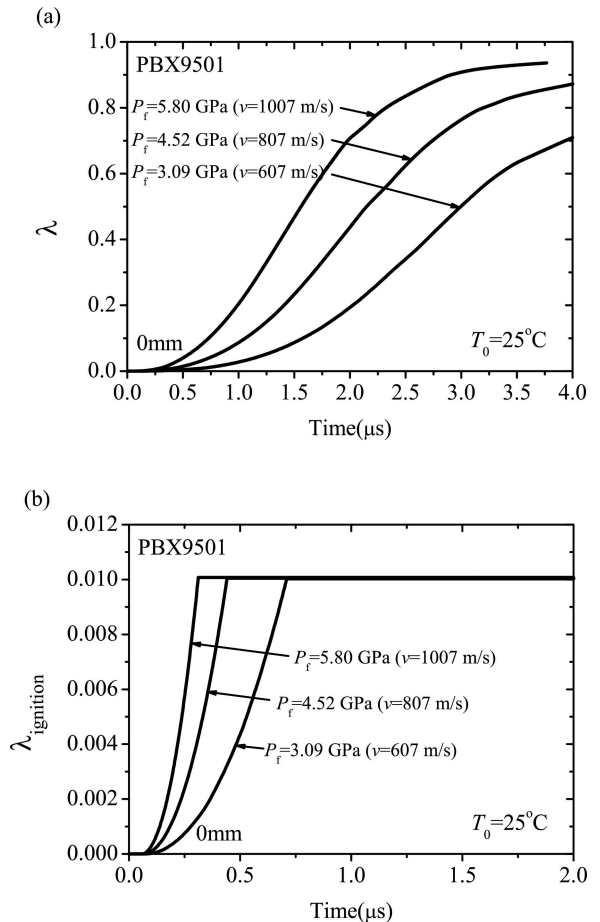


Figure 5. Effects of shock loadings on the shock initiation of PBX9501. (a) Overall reaction degree histories at 0 mm, (b) reaction degree histories of the hot-spot ignition term at 0 mm.

stricted as small as possible to effectively reduce the initiation sensitivity, which is consistent with commonly held ideas.

The calculated Pop-plot for PBX9501 is compared with experimental data in Refs. [26–27,33] in Figure 9. The results show that calculated results by SHS-DZK model give a good match to the experimental data. The run-distance of PBX9501 with a medium density of $\rho_0 = 1.833 \text{ g/cm}^3$ is the shortest, while that for the case of high density of $\rho_0 = 1.840 \text{ g/cm}^3$ is the longest. The reason is that the optimal combustion topology (with the maximum burning surface area) can be achieved in the explosive with a moderate density, which accelerates the combustion reaction.

5 Conclusions

In this paper, a statistical hot spot reaction rate model is proposed for investigating the shock initiation of PBXs. The effects of mesoscopic void size distribution, shock loadings,

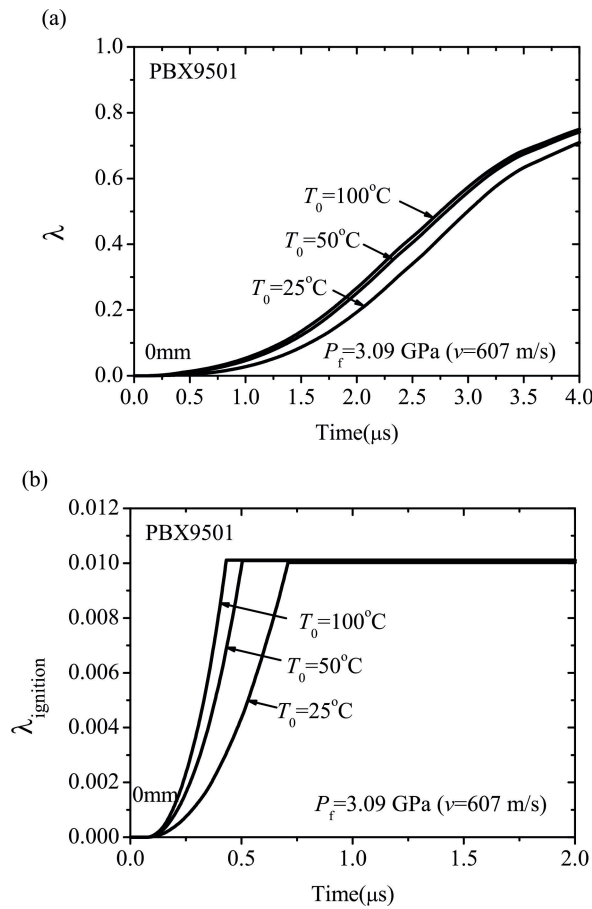


Figure 6. Effects of initial temperature on the shock initiation of PBX9501. (a) Overall reaction degree histories at 0 mm, (b) reaction degree histories of the hot-spot ignition term at 0 mm.

initial temperature were systematically analyzed. The main findings are summarized as follows:

- (1) The shock initiation of HMX-based PBX is mainly controlled by the density of hot spots, and the combustion reacts fast once the hot spot is ignited and shows an accelerated reaction characteristic. While for TATB-based PBX, the critical initiation pressure is high enough to make the reacted hot spots saturated near the shock front and the shock initiation is determined by the combustion reaction, which is characterized by a stable reaction due to the slow combustion-wave velocity. This finding further improves our understanding of the shock initiation mechanism of TATB/HMX-based insensitive high explosives.
- (2) The higher shock loading pressures or higher initial temperature, the smaller critical size of the activated hot spot, the more hot spots generated, and the faster ignition reaction rate. For explosives with the same porosity, the more small voids or the more dispersed the void size, the fewer reactive hot spots generated, and the lower ignition reaction rate. These results suggest

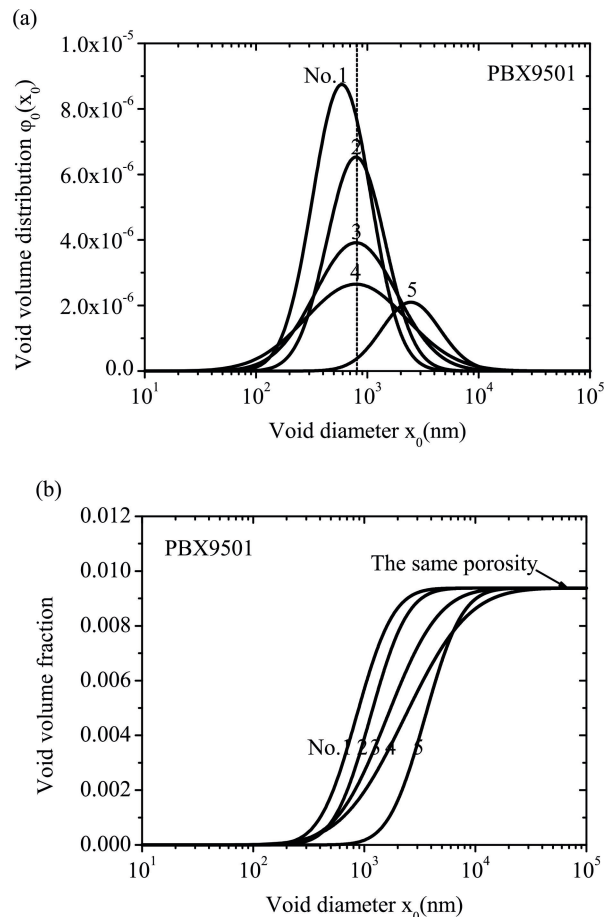


Figure 7. Five different kinds of void size distribution in PBX9501 with the same porosity. (a) Five kinds of void size distribution, (b) having the same porosity.

that the defect size in explosives should be restricted as small as possible to effectively reduce the initiation sensitivity of explosives.

Acknowledgements

This work was supported by the National Natural Science Foundation of China (Grants No. 12002044) and the National Key Laboratory of Shock Wave and Detonation Physics (No. 6142A03192007). The authors thank Prof. Zhen-yu Zhang of National University of Defense Technology for providing the finite element code, DYNA2D, and for assisting in implementing the codes on our system.

Data Availability Statement

The data that support the findings of this study are available from the corresponding author upon reasonable request.

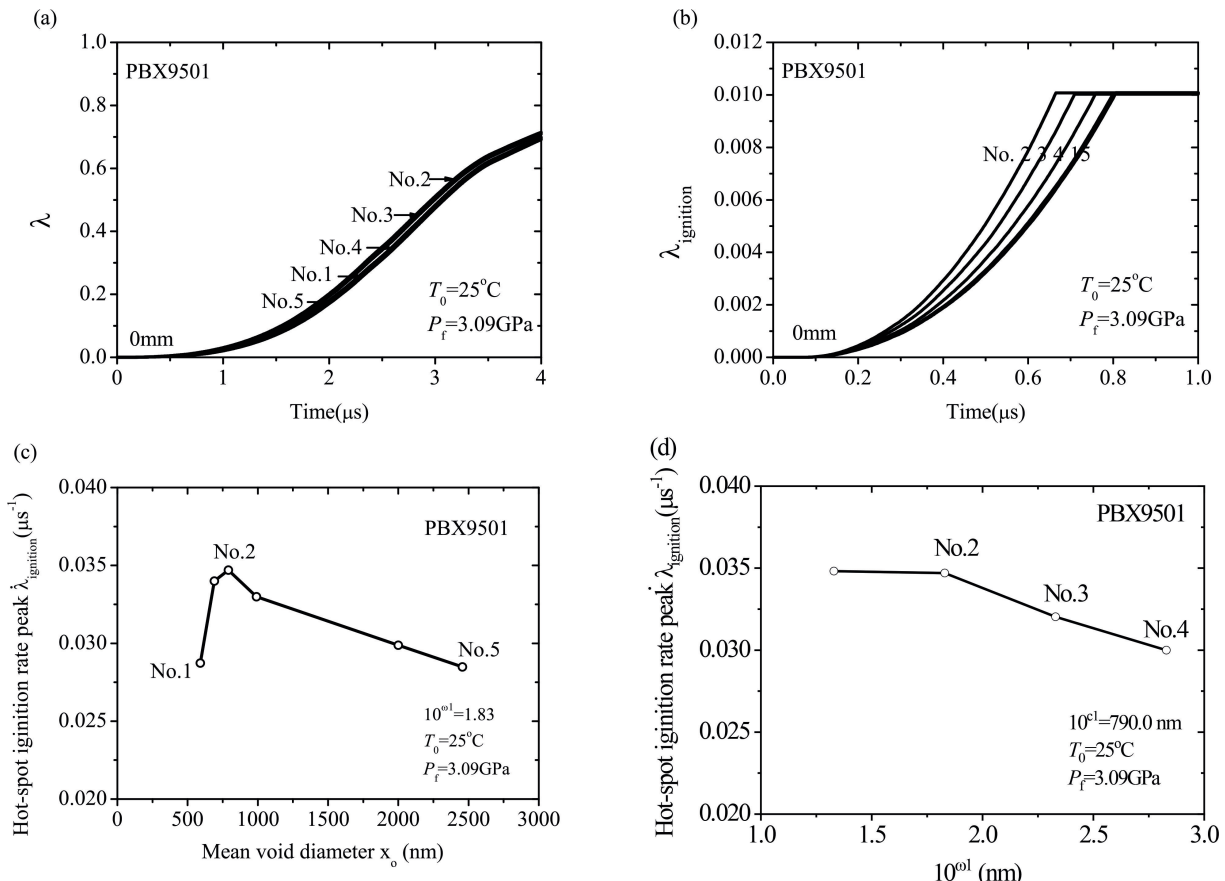


Figure 8. Calculated results showing the effects of void size distribution on the shock initiation of PBX9501. (a) Overall reaction degree histories at 0 mm, (b) hot-spot ignition reaction degree histories at 0 mm, (c) hot-spot ignition rate peak versus the mean void diameter, (d) hot-spot ignition rate peak versus the void size distribution parameter 10^{w1} .

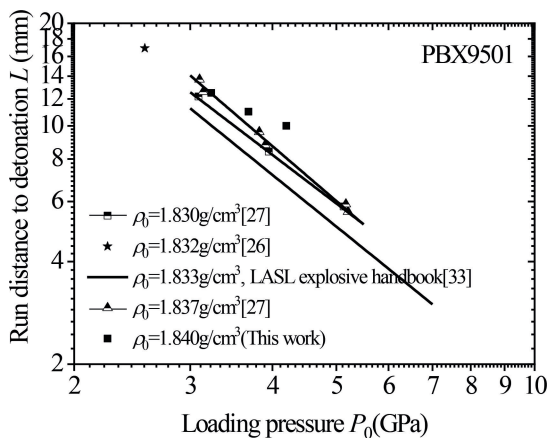


Figure 9. Comparison of calculated and experimental Pop-plot for PBX9501.

References

- [1] R. L. Gustavsen, S. A. Sheffield, R. R. Alcon, J. W. Forbes, C. M. Tarver, F. Garcia, Embedded Electromagnetic Gauge Measure-

ments and Modeling of Shock Initiation in the TATB Based Explosives LX-17 and PBX 9502, *AIP Conf. Proc.* **2002**, 620, 1019–1022. <https://doi.org/10.1063/1.1483711>.

- [2] P. A. Urtiew, C. M. Tarver, Shock Initiation of Energetic Materials at Different Initial Temperatures (Review), *Combust. Explos. Shock Waves* **2005**, 41, 766–776. <https://doi.org/10.1007/s10573-005-0085-0>.
- [3] L. J. Wen, Z. P. Duan, Z. Y. Zhang, Z. C. Ou, F. L. Huang, Experimental research on differences of detonation growth process between HMX-based and TATB-based plastic bonded explosives. *Combust. Explos. Shock Waves* **2013**, s1, 135–139. (in chinese) <https://doi.org/CNKI:SUN:BZCJ.0.2013-S1-024>.
- [4] J. W. Forbes, C. M. Tarver, G. F. Urtiew, The effects of confinement and temperature on the shock sensitivity of solid explosives. 11th International Detonation Symposium, Snowmass, CO, Aug 31-Sep 4; 1998.
- [5] R. N. Mulford, R. R. Alcon, Shock initiation of PBX-9502 at elevated temperatures. American Physical Society biennial conference on shock compression of condensed matter, Seattle, WA (United States), Aug 13–Aug 18; 1995.
- [6] W. L. Perry, B. Clements, X. Ma, J. T. Mang, Relating microstructure, temperature, and chemistry to explosive ignition and shock sensitivity, *Combust. Flame* **2018**, 190, 171–176. <https://doi.org/10.1016/j.combustflame.2017.11.017>.

- [7] P. A. Urtiew, C. M. Tarver, JW. Forbes, G. Garcia, Shock sensitivity of LX-04 at elevated temperatures. Meeting of the topical group on shock compression of condensed matter of the American Physical Society, Amherst, MA (United States), Jul 27-Aug 1;1997.
- [8] R. L. Simpson, P. A. Urtiew, C. M. Tarver, Shock initiation of 1,3,3-trinitroazetidine (TNAZ). *AIP Conf. Proc.* **1996**, 883–886. <https://doi.org/10.1063/1.50587>.
- [9] C. M. Tarver, R. L. Simpson, P. A. Urtiew, Shock initiation of an ϵ -CL-20-estane formulation. *AIP Conf. Proc.* **1996**, 891–894. <https://doi.org/10.1063/1.50589>.
- [10] P. A. Urtiew, C. M. Tarver, R. L. Simpson, Shock initiation of 2,4-dinitroimidazole (2,4-DNI). *AIP Conf. Proc.* **1996**, 887–890. <https://doi.org/10.1063/1.50588>.
- [11] B. A. Khasainov, B. S. Ermolaev, H. N. Presles, P. Vidal, On the effect of grain size on shock sensitivity of heterogeneous high explosives, *Shock Waves* **1997**, 7, 89–105. <https://doi.org/10.1007/s001930050066>.
- [12] L. J. Wen, Z. P. Duan, L. S. Zhang, Z. Y. Zhang, Z. C. Ou, F. L. Huang, Effects of HMX Particle Size on the Shock Initiation of PBXC03 Explosive, *Int. J. Nonlin. Sci. Num.* **2012**, 13, 189–194. <https://doi.org/10.1515/ijnsns.2011.129>.
- [13] H. Moulard, A. Delclos, J. Kury, The effect of RDX particle size on the shock sensitivity of cast PBX formulations: 2, Bimodal compositions, International symposium on pyrotechnics and explosives, Beijing, China, Oct 12; 1987.
- [14] T. M. Willey, T. V. Buuren, J. R. I. Lee, G. E. Overturf, J. H. Kinney, J. Handly, B. L. Weeks, J. Ilavsky, Changes in Pore Size Distribution upon Thermal Cycling of TATB-based Explosives Measured by Ultra-Small Angle X-Ray Scattering, *Propellants Explos. Pyrotech.* **2010**, 31, 466–471. <https://doi.org/10.1002/prep.200600063>.
- [15] Y. R. Liu, Z. P. Duan, Z. Y. Zhang, Z. C. Ou, Huang FL. A mesoscopic reaction rate model for shock initiation of multi-component PBX explosives, *J. Hazard. Mater.* **2016**, 317, 44–51. <https://doi.org/10.1016/j.jhazmat.2016.05.052>.
- [16] Z. P. Duan, L. J. Wen, Y. R. Liu, Z. C. Ou, F. L. Huang, Z. Y. Zhang, A Pore Collapse Model for Hot-spot Ignition in Shocked Multi-component Explosives, *Int. J. Nonlin. Sci. Num.* **2010**, 11, 19–24. <https://doi.org/10.1515/IJNSNS.2010.11.S1.19>.
- [17] Z. L. Bai, Z. P. Duan, L. J. Wen, Z. Y. Zhang, Z. C. Ou, F. L. Huang, Comparative Analysis of Detonation Growth Characteristics between HMX- and TATB-based PBXs, *Propellants Explos. Pyrotech.* **2019**, 44, 858–869. <https://doi.org/10.1002/prep.201800390>.
- [18] Z. L. Bai, Z. P. Duan, L. J. Wen, Z. Y. Zhang, Z. C. Ou, F. L. Huang, Shock initiation of multi-component insensitive PBX explosives: Experiments and MC-DZK mesoscopic reaction rate model, *J. Hazard. Mater.* **2019**, 369, 62–69. <https://doi.org/10.1016/j.jhazmat.2019.02.028>.
- [19] Z. L. Bai, Z. P. Duan, L. J. Wen, Z. Y. Zhang, Z. C. Ou, F. L. Huang, Embedded Manganin Gauge Measurements and Modeling of Shock Initiation in HMX-Based PBX Explosives with Different Particle Sizes and Porosities, *Propellants Explos. Pyrotech.* **2020**, 45, 908–920. <https://doi.org/10.1002/prep.201900376>.
- [20] C. M. Tarver, J. O. Hallquist, L. M. Erickson, Modeling short pulse duration shock initiation of solid explosives, 8th International Detonation Symposium, Albuquerque, NM, USA, Jul 15-Jul 19; 1985.
- [21] K. F. Grebenkin, Comparative analysis of physical mechanisms of detonation initiation in HMX and in a low-sensitive explosive (TATB). *Combust. Explos. Shock Waves* **2009**, 45, 78–87. <https://doi.org/10.1007/s10573-009-0011-y>.
- [22] S. G. Cochran, Statistical treatment of heterogeneous chemical reaction in shock-initiated explosives, Technical Report :UCID-18548; 1980.
- [23] A. L. Nichols, C. M. Tarver, A Statistical Hot Spot Reactive Flow Model for Shock Initiation and Detonation of Solid High Explosives. 12th International Detonation Symposium, San Diego, CA (US), Aug 11-Aug 16; 2002.
- [24] J. R. Gambino, A. L. Nichols, A morphologically aware model for TATB based explosives. *AIP Conf. Proc.* **2020**, 2272, 030011. <https://doi.org/10.1063/12.0000871>.
- [25] L. Hill, The Shock-Triggered Statistical Hot Spot Model. *AIP Conf. Proc.* **2012**, 1426, 307–310. <https://doi.org/10.1063/1.3686280>.
- [26] Y. Hamate, Y. Horie, Ignition and detonation of solid explosives: a micromechanical burn model. *Shock Waves* **2006**, 16, 125–147. <https://doi.org/10.1007/s00193-006-0038-x>.
- [27] Y. Hamate, Y. Horie, A Statistical Approach on Mechanistic Modeling of High-Explosive Ignition. *AIP Conf. Proc.* **2004**, 706, 335–338. <https://doi.org/10.1063/1.1780247>.
- [28] Z. L. Bai, Physical Mechanism and Series of Chemical Reaction Rate Models for Detonation Initiation in PBX explosives. Beijing: Beijing Institute of Technology; 2019.
- [29] J. T. Mang, R. P. Hjelm, E. G. Francois, Measurement of Porosity in a Composite High Explosive as a Function of Pressing Conditions by Ultra-Small-Angle Neutron Scattering with Contrast Variation. *Propellants Explos. Pyrotech.* **2010**, 35, 7–14. <https://doi.org/10.1002/prep.200900026>.
- [30] Z. D. Tian, Z. Y. Zhang, A mesomechanic model of shock initiation in PBX-9404 explosive, *Chin. J. Energet. Mater.* **2007**, 15, 464–467. (in chinese) [https://doi.org/10.1016/S1001-6058\(07\)-60030-4](https://doi.org/10.1016/S1001-6058(07)-60030-4).
- [31] R. Landshoff, A numerical method for treating fluid flow in the presence of shocks, Technical Report LA-1930, Los Alamos Natl. Lab. **1955**.
- [32] P. A. Urtiew, K. S. Vandersall, C. M. Tarver, Initiation of Heated PBX-9501 Explosive When Exposed to Dynamic Loading, Zababakhin Scientific Talks, UCRL-CONF-214667, Snezhinsk, Russia, Sep 05 - Sep 10; 2005.
- [33] T. R. Gibbs, A. Popolato, J. F. Baytos, *LASL explosive property data*[M]. Berkeley: University of California Press, 1980.

Manuscript received: April 18, 2021

Revised manuscript received: June 18, 2021

Version of record online: September 29, 2021